Scanning tunneling spectroscopy of dislocations in ultrathin fcc and hcp Co films

M. Pratzer and H. J. Elmers*
Universität Mainz, Institut für Physik, D-55128 Mainz, Germany
(Received 9 December 2004; published 28 July 2005)

Co grows on W(110) in close-packed layers with hcp and fcc stacking. During further growth, the corresponding stacking faults result in dislocations at the boundaries of coalescing islands. Using scanning tunneling spectroscopy, we could distinguish between different types of dislocations, which in turn are related to dislocation types modeled with hard spheres. In contrast to the hard sphere model, the dislocations in the Co film extend over several unit cells. Therefore, the average atomic density becomes the main distinguishing parameter. The change of the electronic structure in the dislocation with respect to homogeneous films is characterized by a shift of electronic states towards higher binding energy.

DOI: 10.1103/PhysRevB.72.035460 PACS number(s): 73.20.−r, 73.40.Gk, 68.37.Ef, 73.20.At

I. INTRODUCTION

The occurrence of stacking fault dislocations is a regularly observed phenomenon for crystal growth of close-packed structures in (111) orientation when the growth proceeds far from the thermodynamic equilibrium, i.e., for vacuum thin-film growth.[1] On the close-packed surfaces fcc(111) and hcp(0001), adatoms can adsorb on two nonequivalent threefold hollow adsorption sites, thus resulting in fcc- or hcp-like stacking sequences. In many systems, the adsorption energy is similar for both inequivalent sites and further growth leads to twin crystallite formation, forming dislocations at the boundaries. Recently, an understanding of the underlying atomic processes was achieved in the model system Ir/Ir(111).[2] The equilibrium distribution of small clusters between hcp and fcc sites is frozen by the attachment of immobilizing adatoms during growth.

The presence of stacking faults and dislocations in thin films has an intense influence on their electronic properties, particularly for magnetic multilayers.[3] For magnetic films, the uniaxial symmetry of the hcp structure can induce a magnetic anisotropy that is absent in the corresponding fcc film. For example, Co/W(110) (See Ref. 4) and Co/Mo(110) (See Ref. 5) films with a preferred hcp structure exhibit a bulk-like contribution to the magnetic anisotropy favoring an easy axis perpendicular to the surface, while for Co/Cu(111) films with a preferred fcc structure,[6] magnetocrystalline contributions to the magnetic anisotropy can be neglected.[7] The role of the stacking sequence on magnetic anisotropies has been explained by theoretical models.[8] For tunneling magnetoresistive devices, transport properties are largely governed by electronic interface states.[9] For close-packed Co surfaces, these interface states crucially depend on the stacking sequence as has been observed for Co/Cu(111)[10–12] and Co/W(110)[13,14] films by scanning tunneling spectroscopy (STS). *Ab initio* calculations reveal that the stacking sequence strongly changes a $d_{3z^2-r^2}$-like surface resonance at −0.3 eV below the Fermi energy.[14]

Dislocations that are formed during growth at the boundaries of coalescing crystallites with different stacking sequences provide a unique contribution to the properties of films and multilayers. Dislocations may severely change the oscillating indirect exchange coupling.[15] Controversial results on the presence or absence of antiferromagnetic coupling observed for Co/Cu(111) multilayers[16,17] were explained by different densities of stacking faults in the Cu(111) interlayers. If the dislocations at the boundaries of Cu crystallites were filled by Co atoms during further growth of the multilayer, these Co atoms would provide a direct ferromagnetic coupling and thus mask the weak antiferromagnetic coupling.[15,18] Besides this morphological influence, stacking fault dislocations may show an electronic structure different from homogeneous crystallites. This question was recently addressed by Wiebe *et al.*[14] For dislocations in Co/W(110) films that were formed near the substrate interface and then buried by additional Co layers, no significant difference was found.

In this paper, the development of dislocations in ultrathin Co films on W(110) is described for a coverage of up to 3 monolayers (ML). The Co/W(110) system serves here as a model system, because interface alloying is suppressed and the stacking sequence can be determined unambiguously for islands up to a 3 ML thickness. We present a systematic classification of the various possible dislocation types based on a hard sphere model, in extension of the classification scheme given by Busse *et al.*[2,19] for the case of Ir/Ir(111). In contrast to the Ir/Ir(111) system, the stiffness is much smaller in Co films and consequently dislocations are strain relaxed over several unit cells. The altered local density of atoms causes changes in the electronic structure, which is investigated by scanning tunneling spectroscopy.

II. EXPERIMENT

The experiments were carried out using an ultrahigh vacuum chamber ($p<1\times10^{-10}$ Torr). The single-crystal W(110) surface was cleaned by cycles of annealing in an oxygen atmosphere and subsequent flashing at 2000 K. Cobalt was evaporated with a rate of 0.1 ML/min at substrate temperatures of approximately 420 K from a BeO crucible using a homebuilt evaporator. The substrate temperature was varied slightly in order to adjust the island sizes. The pressure increases during Co evaporation to $p=2\times10^{-10}$ Torr. The cleanliness of the samples was checked by Auger spec-

troscopy. STS was performed to obtain differential conductance dI/dU maps and spectra, using a lock-in technique with a 8 kHz bias voltage modulation of 30–50 mV. All bias voltages given are sample voltages with respect to the tip. The data shown here are measured using a $Pt_{80}Ir_{20}$ tip that was cut under tensile stress from a thin wire. Spectroscopic measurements were done directly after the sample preparation with residual gas exposures less than 0.5 L (10^{-6} Torr s).

III. HARD SPHERE MODEL

The first Co layer grows initially as a pseudomorphic monolayer on W(110). During further growth the pseudomorphic monolayer transforms into a close-packed layer, which remains pseudomorphic along the bcc$[1\bar{1}0]$ direction. Thus, dislocations in the first Co layer are suppressed. If the first layer is denoted by A, the second layer may grow in two different positions relative to layer A, denoted as B and C. The trilayer (TL) then may have a fcc stacking (ABC or ACB), or a hcp stacking (ABA or ACA). Areas with fcc stacking can be distinguished with STS from areas with hcp stacking because of the different electronic structure.[13] The different stackings AB and AC in the bilayer (BL) are symmetrically equivalent to each other and therefore show no spectroscopic difference. However, islands with AB and AC stacking are separated by dislocation lines that might be seen in STS images.

An illustrative explanation for the occurrence of different types of dislocations is given by the hard sphere model of close-packed structures. Figure 1 shows BL and TL islands with all possible stacking sequences. The boundaries of the Co islands are preferably oriented along the hcp $[10\bar{1}0]$, $[0\bar{1}10]$, and $[\bar{1}100]$ directions, thus forming closely packed edges. For the BL islands two different types of steps can be identified at the boundaries. In the top view shown in Fig. 1, the edge atoms of a BL island form a rectangular unit cell at steps denoted as α and a parallelogram unit cell at steps denoted as β. In our case, steps α and β are energetically equivalent, as seen by the occurrence of hexagonally shaped islands. A considerable energy difference between the two types of steps would result in triangular islands as observed; e.g., for Ir islands on Ir(111).[19] For hexagonal islands as shown in Fig. 1 steps on opposite sides of an island are always complementary to each other. For coalescing islands dislocation lines are formed, if similar steps approach each other. Consequently, two inequivalent dislocations are formed, which we denote as $\alpha-\alpha$ and $\beta-\beta$. The dislocations can be characterized by the distance of atomic rows in the second layer, i.e., by the width of the groove, as indicated in Fig. 5(a):

$$d_{\alpha-\alpha} = \frac{4}{3}\frac{\sqrt{3}}{2}a_{\mathrm{Co}} \approx 0.289[\mathrm{nm}],$$

$$d_{\beta-\beta} = \frac{5}{3}\frac{\sqrt{3}}{2}a_{\mathrm{Co}} \approx 0.362[\mathrm{nm}]. \quad (1)$$

If an α step meets a β step, the distance of the atomic rows will be given by $d_0=(\sqrt{3}/2)a_{\mathrm{Co}} \approx 0.217$ nm, corresponding to the row distance in the close packed structure without dislocations. Therefore, the extra distance at the dislocations is $d_{\alpha-\alpha}-d_0 \approx 0.072$ nm and $d_{\beta-\beta}-d_0 \approx 0.145$ nm.

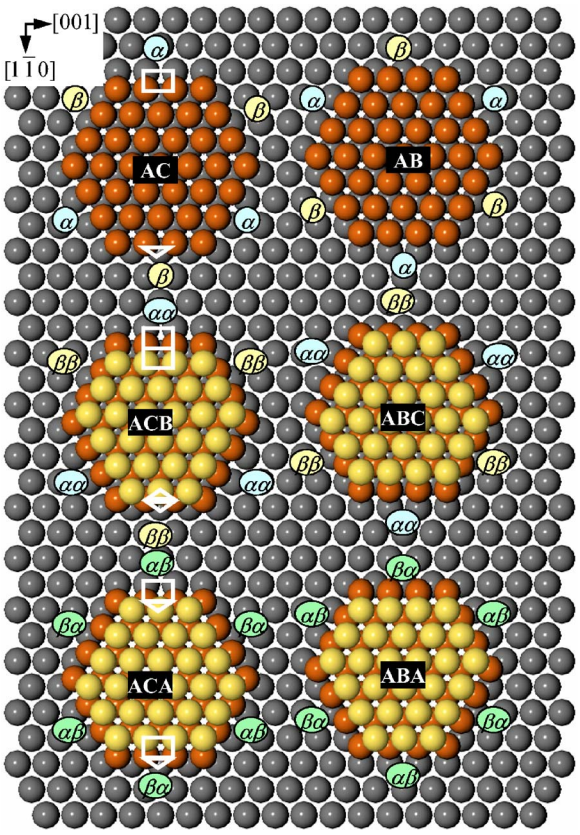

FIG. 1. (Color online) Hard sphere model of close-packed bilayer and trilayer islands on a close-packed layer in (111) orientation. BL and TL islands are shown for all possible stacking sequences, assuming the lowest layer being an A layer. The different types of steps are denoted by italic letters. For hexagonal islands the steps on opposite edges are complementary to each other.

The double steps occurring at the boundaries of bilayer islands on the first close-packed layer (TL islands) are consequently denoted by two letters. The four different types of steps are denoted as $\alpha\alpha$, $\beta\beta$, $\alpha\beta$, and $\beta\alpha$. A particular TL island reveals only the combinations $\alpha\alpha$ with $\beta\beta$ and $\alpha\beta$ with $\beta\alpha$ as pairs of complementary types of steps. According to the combination of step types at dislocation lines formed at coalescing TL islands, basically 16 different types of dislocations may occur. However, the four combinations $\alpha\alpha-\beta\beta$, $\beta\beta-\alpha\alpha$, $\alpha\beta-\beta\alpha$, and $\beta\alpha-\alpha\beta$ cancel each other because they belong to islands with the same stacking sequence. The remaining 12 combinations form true dislocations. These 12 different types are shown in Fig. 2, ordered by systematic variation of step types. Two complementary dislocations for a particular pair of islands are shown in one row. The dislocation types are summarized in Table I, ordered by the variation of stacking sequences.

As in the case of BL islands, the dislocations in TL islands are characterized by the distance between atomic rows at the dislocation in the second (D_{BL}) and third layer (D_{TL}) which may assume values of 3 (for no dislocation), 4, and 5 in units of $a_{\mathrm{Co}}/(2\sqrt{3})$ (see Fig. 2 and Table I).

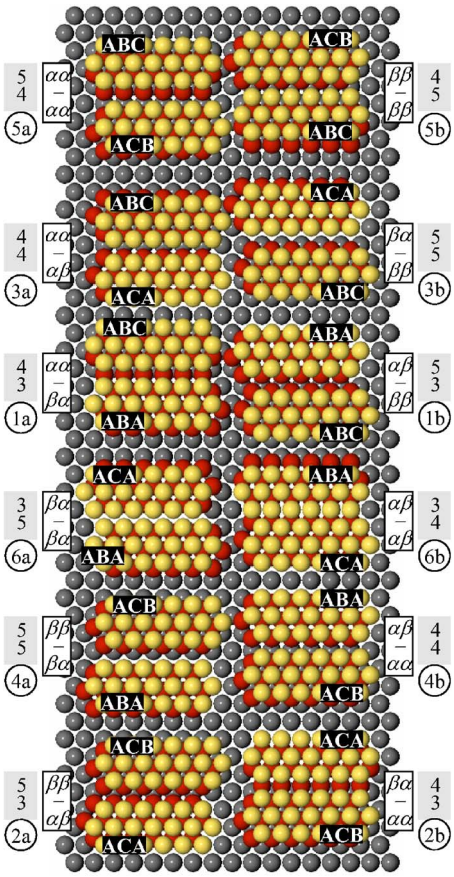

FIG. 2. (Color online) Hard sphere model of all possible dislocation types in TL films with a common base layer. Complementary dislocation types are shown in a row. The dislocations are characterized by the distance of atomic rows in the second and third layer at the dislocation line D_{BL} and D_{TL}, given in units of $d_0/3$. The complementary dislocation types are denoted as described in Table I.

IV. EXPERIMENTAL OBSERVATIONS

In principle, dislocations should be visible in a topographical STM image (see, e.g., Ref. 2). However, for ultrathin Co films on W(110) it has been shown previously that the dislocations can be hardly detected.[13,14] This is different for STS images (dI/dU maps), where the spectroscopic contrast can be exploited to observe the dislocations. Figure 3 shows a series of dI/dU maps taken for varying sample voltages at the same probe area. The probe area comprises a TL island with fcc stacking in the bottom right corner of the island and hcp stacking elsewhere. The fcc stacking shows up as a bright area for sample voltages close to −0.4 V and +0.3 V in agreement with previous observations.[13] For sample voltages between −0.65 V and 0.45 V, a bright line appears at the borderline between fcc and hcp areas, indicating the dislocation. A reversed contrast shows up for sample voltages between −0.25 V and −0.1 V and also between +0.1 V and 0.2 V, where the dislocation results in a dark line. The largest contrast appears at sample voltages −0.45 V and −0.4 V, which have been used in the following. The dislocation contrast depends on the in-plane direction of the dislocation line. While the dislocation is clearly visible at the left boundary of the fcc area, the contrast is faint at the upper boundary line that has a large angle with respect to [001] (indicated by arrows in Fig. 3).

Figures 4(a) and 4(b) show a TL island consisting of a large hcp area in the center surrounded by smaller fcc areas. The borderline between fcc and hcp areas is clearly different at the upper and lower boundary of the hcp area. While the upper dislocation shows up as a bright line, the lower dislocation fails to show a spectroscopic contrast. The occurrence of complementary dislocations can be nicely observed for the elongated island shown in Figs. 4(e) and 4(f), comprising alternating areas of hcp and fcc stacking. Reading from the left edge, the hcp/fcc transition appears always dark while the fcc/hcp transition appears always bright. As motivated by the hard sphere model, complementary dislocations are expected at opposite boundaries of the hcp area. Surprisingly, the dislocation line always appears either bright or dark, with only a small variation of the spectroscopic contrast depending on the angle between the [001] direction and the dislocation line. This observation can be explained by the fact that the threefold symmetry of the fcc (111) surface is broken in our case. Because of the misfit of the Co bulk lattice with respect to the substrate along $[1\bar{1}0]$ of $f_i=(b_i-a_i)/a_i=-0.032$ ($i=[1\bar{1}0]$, b_i and a_i denoting corresponding lengths

TABLE I. Types of dislocations formed at coalescing BL (0a and 0b) and TL (1a–6b) islands of different stacking sequences. Because of mirror symmetry type 1a is equivalent to 2b. The same equivalence holds for 2a and 1b, 3a and 4b, and 4a and 3b. Dislocations between two fcc stackings (5a and 5b) require a dislocation in each of the topmost layers, while at dislocations between hcp stackings (6a and 6b), only the center layer shows the dislocation. Dislocations that show up as a bright line (at $U=-0.45$ V) are indicated by +, the complementary dislocation by −. Type 5 dislocations could not be clearly identified.

		a	D_{BL}	D_{TL}		b	D_{BL}	D_{TL}	
0	BL-BL	AB→AC	4	−	(−)	AC→AB	5	−	(+)
1	fcc-hcp	ABC→ABA	3	4	−	ABA→ABC	3	5	+
2	fcc-hcp	ACB→ACA	3	5	+	ACA→ACB	3	4	−
3	fcc-hcp	ABC→ACA	4	4	+	ACA→ABC	5	5	−
4	fcc-hcp	ACB→ABA	5	5	−	ABA→ACB	4	4	+
5	fcc-fcc	ABC→ACB	4	5	0	ACB→ABC	5	4	0
6	hcp-hcp	ACA→ABA	5	3	+	ABA→ACA	4	3	−

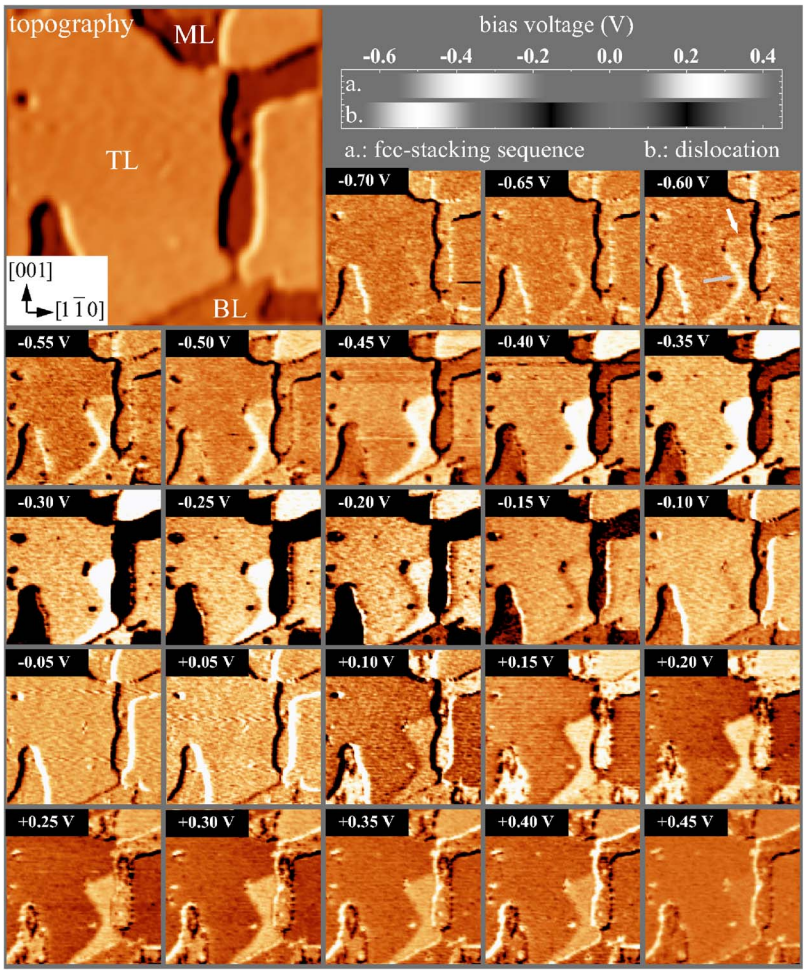

FIG. 3. (Color online) Series of dI/dU maps [(50×50) nm^2] of a TL island comprising both hcp and fcc stacking for sample voltages as indicated in each image ($I=0.6$ nA). A topographic image of the same area is shown in the upper left corner. The intensity diagram shown at the top qualitatively reflects the dI/dU intensity as a function of the sample voltage for fcc areas (a) and at the dislocation (b) indicated by the blue (gray) arrow. For $U=-0.6$ V, the dI/dU intensity depends on the crystallographic direction of the dislocation line (indicated by the blue (gray) and yellow (white) arrows).

of adsorbate and substrate unit cells), the resulting epitaxial strain leads to a preferential orientation of island edges along [001], thus favoring steps with the closest packing.[13] Consequently, the preferred orientation of dislocation lines is along [001], too. Deviations of the dislocation direction from [001] will be adopted by small sections of only a few unit cells along an energetically unfavorable direction separating comparatively long sections along [001]. Because the deviation of the electronic structure at the dislocation extends over several unit cells, the short dislocation sections along unfavorable directions remain undetectable. From the observation of many (bright) dislocation lines, one finds a decrease in intensity with decreasing deviation from the [001] direction.

Figure 4(c) shows a line scan across the (bright) dislocation. If the difference in the dI/dU signal for fcc and hcp areas is subtracted by a step function, the deviation caused by the dislocation can be described remarkably well by a Gaussian function. The full width at half-maximum value of 1.85 nm means that the deviation of the electronic structure extends over a much larger area than suggested by the hard sphere model. The most probable explanation is a strain relaxation of dislocations; i.e., all atoms in the vicinity of the dislocation are displaced in such a way that close-packed unit cells are formed locally. This assumption is further supported by the observation of an atomically resolved dislocation network in thicker Co/W(110) films with a width of 3 nm for individual dislocation lines.[14]

The prominent difference in the dI/dU spectra between the (bright) dislocation and homogeneous areas of fcc stacking appears as a shift of the peak at −0.4 V by (50±20) mV towards higher binding energies for the dislocation [see Fig. 4(d)]. The dI/dU spectra have been taken after stabilizing the tip position with $U=1$ V at $I=0.5$ nA. Thus, the tip is positioned for the spectroscopic measurement at a larger tip-sample distance compared to the conditions for measuring dI/dU maps. Nevertheless, the shift of the peak position can also be qualitatively observed in the series of STS images (see Fig. 3).

For BL areas, only two different types of dislocation exist: $\alpha-\alpha$ and $\beta-\beta$. Denoting the first Co layer as an A layer, the $\alpha-\alpha$ dislocation occurs at a transition from AB to AC stacking (from top to bottom) for dislocation orientation along [001] [see Fig. 5(a)]. According to our notation, we refer to the $\alpha-\alpha$ ($\beta-\beta$) dislocation as a 0a (0b) dislocation, and the distance of atomic rows at the dislocation is $4\times a_{\mathrm{Co}}/(2\sqrt{3})$ [$5\times a_{\mathrm{Co}}/(2\sqrt{3})$]. Although only one pair of complementary dislocations exists, the experimental observation is not that simple. Figures 5(b) and 5(c) show a STM and corresponding STS image of a BL area for a sample voltage of $U=-0.45$ V. The dislocation lines, indicated by the arrows, show up as alternating dark and bright lines separating areas of AB and AC stacking with a preferential orientation along [001]. In this case, we observe a sequence of complementary dislocations, as expected from the hard sphere model. How-

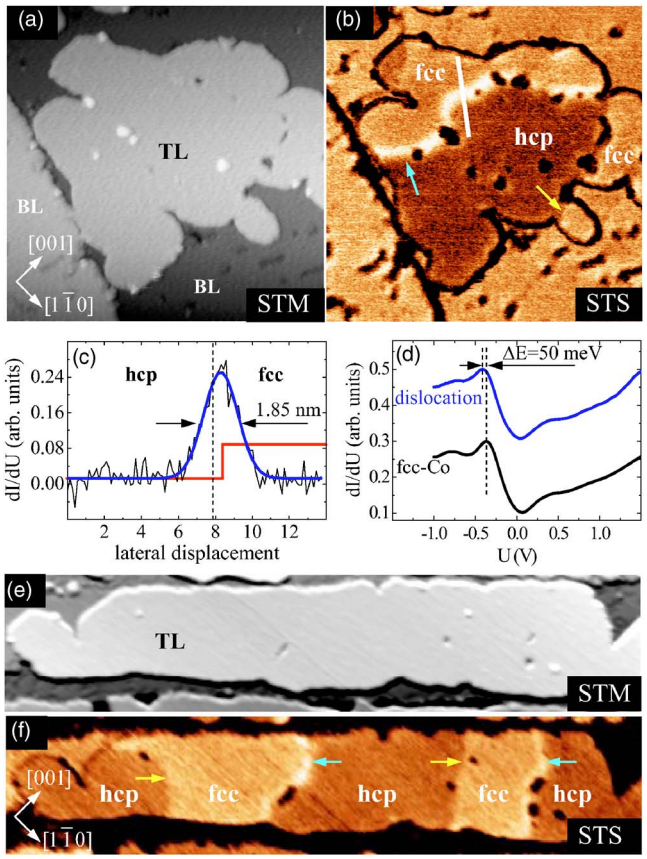

FIG. 4. (Color online) (50×50) nm^2 STM (a) and STS images (b) of a TL Co island ($U=-0.4$ V, $I=0.55$ nA), comprising a central hcp area surrounded by fcc areas. Two types of dislocations can be distinguished. The lower dislocation, indicated by the arrow shows no additional spectroscopic feature, while the upper dislocation is indicated by a prominent bright line. The line scan (c) across the bright dislocation is fitted by a Gaussian function after subtraction of a step function. (d) dI/dU spectra (stabilization parameters $U=1$ V, $I=0.5$ nA) measured at the dislocation (upper spectra) and on a homogeneous fcc area (lower spectra). The peak at $U=-0.4$ V is shifted towards higher binding energies on the dislocation. (e) (130×30) nm^2 STM image of a TL Co stripe ($U=-0.4$ V, $I=0.7$ nA) and corresponding STS image (f). Alternating hcp and fcc areas lead to alternating occurrence of complementary dislocation types.

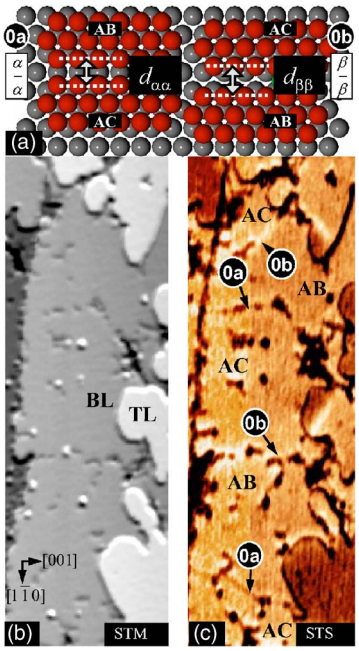

FIG. 5. (Color online) (a) Hard sphere model of the dislocation along [001] in BL islands. (b) (30×90) nm^2 STM image of a BL Co stripe ($U=-0.45$ V, $I=0.6$ nA) and corresponding STS image (c). The alternating appearance of complementary dislocation types (narrow dark lines and wider bright lines indicated by 0a and 0b, corresponding to the dislocation type) separate alternating stacking sequences AB and AC. Black spots are caused by adsorbed molecules from the residual gas.

ever, in many STS images the BL dislocations could not be observed at $U=-0.45$ V. Instead, a dark line appears at $U=+0.3$ V for the 0a (BL) dislocations [see Fig. 7(b)]. In some cases the BL dislocations could not be clearly identified.

The black dots in Fig. 5(c) indicate spots where the dI/dU signal is very small and therefore may be identified as adsorbed molecules from the residual gas; i.e., CO molecules. These molecules adsorb preferentially at the dislocations. An analysis of several STS images reveals that they adsorb with a higher probability at a dislocation line that shows up with a high dI/dU intensity at $U=-0.45$ V. One expects the adsorbing probability to be higher for the case of a wider dislocation groove; i.e., the 0b dislocation. Therefore, we tentatively assign the dislocation with the high dI/dU intensity at $U=-0.45$ V as the 0b dislocation. This assumption could only be verified by an analysis of atomically resolved dislocations, which was not possible in our case.

Starting from our tentative assignment of the relative atomic positions in bilayer areas, stacking sequences in TL areas and, consequently, dislocation types can be determined, as well. Therefore, one has to analyze overgrowing layers at substrate steps. This is illustrated in Fig. 6, where topographical and spectroscopic information is combined for a sample area comprising four terraces covered by one, two, or three atomic layers of Co. In this figure, BL areas appear bright, ML areas dark, and TL areas dark or bright depending on the stacking sequence.

The position of the first Co layer on the second terrace (from the top) is defined as an A layer. AB and AC stackings of the BL are identified as described above. The BL dislocation 0b, indicated by the mark b) in Fig. 6 is completely covered by molecules. Considering, e.g., the continuation of the AB stacking from the second to the third terrace indicated by the mark a) in Fig. 6, the stacking sequence must be BAB on the third terrace because it is an hcp island. This hcp area is separated from an adjacent hcp area on the same terrace by a bright dislocation line. Consequently, this adjacent area comprises the stacking sequence BCB. However, the stacking sequence BCB does not match the AB or AC stacking in the adjacent upper terrace. Therefore, overgrowing is avoided in this area. According to Table I, the indicated hcp-hcp dislocation is a 6a dislocation. It could be expected that it appears bright because the dislocation in the center

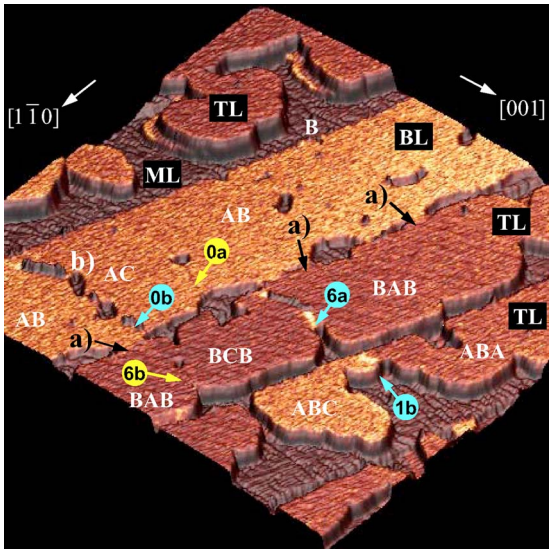

FIG. 6. (Color online) Three-dimensional topographic representation of four W(110) substrate terraces covered by a mean thickness of 3 ps ML Co [(200×200) nm^2]. The surface was colored according to the dI/dU intensity at $U=-0.45$ V and $I=0.6$ nA. The position of the first Co layer on the second terrace (from the top) is defined as an A layer. Areas where the Co coverage is continued (overgrowing) at the substrate step from the second to the third terrace are denoted by (a). At the substrate step from the third to the fourth terrace the topmost layer is discontinued but no extended groove shows up at this step. Therefore, the first two layers on the third terrace are continued on the fourth terrace.

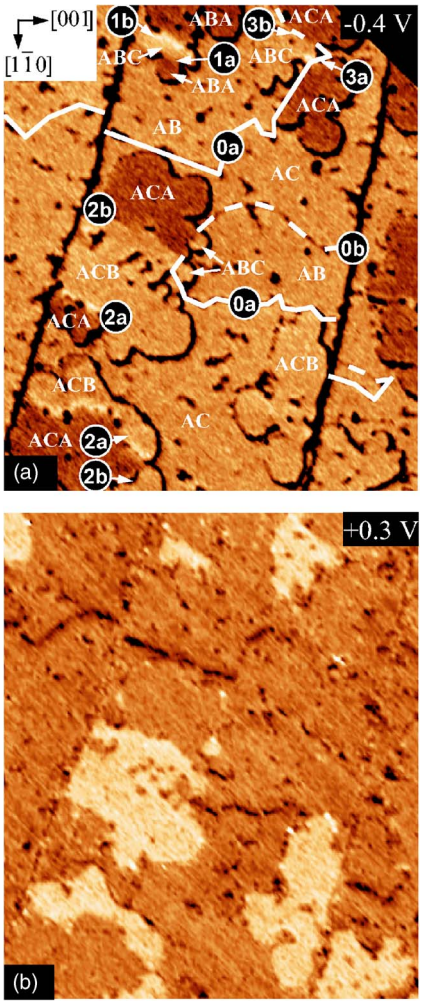

FIG. 7. (Color online) $(145\times160$ nm$^2)$ STS image for sample voltages $U=-0.4$ V (a) and $U=+0.3$ V (b). In the STS image (b), 0a (BL) dislocations show up as dark lines. 0b (BL) dislocations can be identified indirectly by adsorbed molecules. The position of 0a (dotted) and 0b (dashed) dislocations are indicated in (a).

layer has a similar edge formation ($\beta-\beta$) as the dislocation 0b (BL), which appears in some cases bright (see Fig. 5(c)) also. At the left side of the third terrace the overgrowing layers from the second terrace indicate again a BAB stacking sequence. The dislocation is accordingly of type 6b. No significant spectroscopic feature is visible at this dislocation.

Because the two lower layers on the third terrace (Fig. 6) are continued across the substrate step on the fourth terrace, the hcp islands comprise the stacking sequence ABA, while the fcc island is ABC. The type 1b dislocation between fcc and hcp shows up as a bright line. This can again be expected since the dislocation in the topmost layer is of the type $\beta-\beta$ as in the case of types 6a and 0b. The complementary dislocation 1a is avoided in this case because the left hcp area is separated from the fcc island. Note, that the dislocation 0a on the second terrace has finally induced the dislocation 1b on the fourth terrace.

Dislocations on larger terraces can be analyzed similarly. Figure 7 shows STS images for sample voltages $U=-0.4$ V and $U=+0.3$ V at the same sample area. For $U=+0.3$ V, TL islands with fcc stacking show up as white areas, while for $U=-0.4$ V hcp islands appear dark. At $U=+0.3$ V the BL dislocations of type 0a can be identified as a prominent dark line, while the complementary type 0b can be identified only indirectly by adsorbed molecules. The position of the BL dislocation is transferred Fig. 7(b) to Fig. 7(a). Above the upper 0a (BL) dislocation the initial AB stacking sequence results in the ABA sequence of the top-left hcp island. The adjacent fcc island below thus has ABC stacking and the dislocation in between is of type 1b. The complementary type 1a can be found between the fcc island and the small hcp island below. As in this case, most of the TL dislocations occur in the topmost layer.

Below the upper 0a (BL) dislocation the initial stacking sequence is AC. Therefore, the hcp area just below this BL dislocation comprises a ACA sequence separated from the fcc area with ACB stacking by a dislocation of type 2b (see Table I). At the bottom of this large TL island a small hcp area with ACA stacking occurs and the dislocation in between is of type 2a. The same type can also be found on the TL island at the bottom left of Fig. 7(a). The 2a dislocation can be seen as a bright line, which is not surprising since the 2a dislocation is equivalent to the 1b dislocation by symmetry reasons.

The 0a (BL) dislocation in the center of Fig. 7(a) is apparently continued to the left across the left fcc island. The resulting dislocation would be a 5a dislocation with no distinctive spectroscopic feature. Because we never observed a dislocation directly inside an fcc island, it is likely that both types 5a and 5b remain unobtrusive.

A clear indication of a dislocation involving two layers occurs in the top right TL island of Fig. 7(a). It is divided by the continued 0a (BL) dislocation that separates the fcc (ABC) island from the lower hcp (ACA) area, thus forming a 3a dislocation that is bright. The dislocation between the topmost hcp island and the fcc (ABC) island does not show any distinctive spectroscopic feature. If the topmost hcp island had an ABA stacking sequence the corresponding dislocation would be of type 1b and should show up bright, which is not the case. Therefore, we conclude that its stacking is ACA and the dislocation is of type 3b.

From a series of STS images, we find that in most cases TL dislocations are located in just one layer. Dislocation types with dislocations in both layers appear very seldom. This is a consequence of the dynamic growth process, wherein the BL areas coalesce and dislocations are formed in the second layer before the TL islands approach each other. Nucleation of TL islands at the existing BL dislocations may help to avoid the formation of the corresponding dislocations.

Our observation of a dislocation running across a step of the tungsten surface can only be explained if one assumes a long-range interaction between adsorption sites on different terraces. A long-range interaction could be provided by an elastic strain in the W(110) substrate caused by the tensile stress of the epitaxial Co film. Elastic strain in the substrate has indeed been found recently for ultrathin Co/W(110) films by careful x-ray diffraction measurements.[21]

V. CONCLUSION

From the hard sphere model one expects four nonequivalent pairs of complementary dislocations in TL islands: two pairs for fcc-hcp and one pair each for fcc-fcc and hcp-hcp dislocations. From the spectroscopic data at dislocation lines only two groups of dislocation types could be distinguished. The dislocation types 1b, 2a, 3a, 4b, and 6b show the distinctive spectroscopic feature of a small shift of the dI/dU maximum at $U=-0.4$ V by 50 meV towards higher binding energies that results in a bright line in STS images taken at $U=-0.45$ V. In some cases a similar bright line was observed for the 0b (BL) dislocation also. The complementary dislocation types do not show any significant changes in the STS data, except for the 0a (BL) dislocation appearing in some cases as a dark line.

In order to find a common feature of the spectroscopically "active" TL dislocations, we discuss the mean atomic density at the dislocation. Because the dislocations show a significant strain relaxation, the characterization by the mean density of atoms might be adequate. The mean density of a particular dislocation type decreases as the mean distance of atomic rows measured in the hard sphere model increases. Therefore, we denote the dislocation type by the distance of atomic rows D_{BL} in the second layer for BL areas and by the sum of distances in the second and third layer for TL islands $D_{\mathrm{BL}}+D_{\mathrm{TL}}$. The highest density is found for 1a, 2b, 6b, and 0a (BL) dislocations with a mean row distance of $\bar{D}=3.5$, which just exceeds the row distance $\bar{D}=3$ of the regular lattice. The 3b, 4a, 5a, and 5b dislocations show the lowest density with a mean row distance of $\bar{D}=5$ and $\bar{D}=4.5$. This very low density of atoms might be unfavorable and the dislocation can easily be filled by an additional row of atoms, as has been observed for Ir/Ir(111) islands.[20] If the additional row is incorporated into the strained structure, the mean density of the 3b, 4a, 5a, and 5b dislocations will be $\bar{D}=3.25$ and $\bar{D}=3.75$. The remaining 1b, 2a, 3a, 4b, 6b, and 0b (BL) (active) dislocations are characterized by a mean row distance $\bar{D}=4$ and thus exhibit the lowest density.

A shift of electronic states can be expected if the density of atoms is locally changed, but the direction of the shift cannot be predicted absolutely reliable by a simple model. Nevertheless, a shift of electronic surface states towards higher binding energies is likely for the case of decreased atomic density because in a free electron model the kinetic energy decreases for a decreasing wave vector and increasing atomic distance.

Note, that the given identification of dislocations is a tentative one. Starting with the opposite identification for the BL dislocation, the conclusion would be that 1b, 2a, 3a, 4b, 6b, and 0b (BL) dislocations are inactive while 1a, 2b, 3b, 4a, 5a, 5b, 6a, and 0a (BL) dislocations are spectroscopically active. A clearcut identification could be provided by atomically resolved images. However, we could not achieve atomic resolution on such a large area that dislocations could be identified. This is partly a consequence of the dislocations being spread out by strain relaxation (see Ref. 14).

In summary, we found complementary pairs of dislocations in closely packed BL and TL islands with one dislocation of each pair (except for dislocations inside fcc islands) showing up as a bright line in an STS image taken at $U=-0.45$ V. The bright spectroscopic feature is due to a shift of the corresponding electronic state towards higher binding energy. Dislocations are extended over several unit cells, which can be explained by a strain relaxation of dislocations. Obviously, the strain relaxation in Co(111) is much more pronounced compared, e.g., to dislocations observed in Ir(111).

This work was supported by the DFG.

*Electronic address: elmers@uni-mainz.de

[1] M. J. Stowell, *Epitaxial Growth, Part B* (Academic, New York, 1975).

[2] C. Busse, C. Polop, M. Müller, K. Albe, U. Linke, and T. Michely, Phys. Rev. Lett. **91**, 056103 (2003).

[3] U. Gradmann, in *Handbook of Ferromagnetic Materials*, edited by K. H. J. Buschow (Elsevier, Amsterdam, 1993), Vol. 7, p. 11.

[4] H. Fritzsche, J. Kohlhepp, and U. Gradmann, Phys. Rev. B **51**,

15933 (1995).
[5] J. Prokop, D. A. Valdaitsev, A. Kukunin, M. Pratzer, G. Schönhense, and H. J. Elmers, Phys. Rev. B **70**, 184423 (2004).
[6] G. J. Strijkers, J. T. Kohlhepp, H. J. M. Swagten, and W. J. M. de Jonge, Appl. Magn. Reson. **19**, 461 (2000).
[7] J. Kohlhepp, H. J. Elmers, and U. Gradmann, J. Magn. Magn. Mater. **121**, 487 (1993).
[8] J. Dorantes-Davila, H. Dreysse, and G. M. Pastor, Phys. Rev. B **55**, 15033 (1997).
[9] P. LeClair, J. T. Kohlhepp, C. H. van de Vin, H. Wieldraaijer, H. J. M. Swagten, W. J. M. de Jonge, A. H. Davis, J. M. MacLaren, J. S. Moodera, and R. Jansen, Phys. Rev. Lett. **88**, 107201 (2002).
[10] L. Diekhöner, M. A. Schneider, A. N. Baranov, V. S. Stepanyuk, P. Bruno, and K. Kern, Phys. Rev. Lett. **90**, 236801 (2003).
[11] S. N. Okuno, T. Kishi, and K. Tanaka, Phys. Rev. Lett. **88**, 066803 (2002).
[12] A. L. Vazquez de Parga, F. J. Garcia-Vidal, and R. Miranda, Phys. Rev. Lett. **85**, 4365 (2000).
[13] M. Pratzer, H. J. Elmers, Surf. Sci. **550**, 223 (2004).
[14] J. Wiebe, L. Sacharow, A. Wachowiak, G. Bihlmayer, S. Heinze, S. Blügel, M. Morgenstern, and R. Wiesendanger, Phys. Rev. B **70**, 035404 (2004).
[15] J. Kohlhepp, S. Cordes, H. J. Elmers, and U. Gradmann, J. Magn. Magn. Mater. **111**, L231 (1992).
[16] W. F. Egelhoff Jr. and M. T. Kief, Phys. Rev. B **45**, 7795 (1992).
[17] J. P. Renard, P. Beauvillain, C. Dupas, K. LeDang, P. Veillet, E. Velu, C. Marliere, and D. Renard, J. Magn. Magn. Mater. **115**, L147 (1992).
[18] H. J. Elmers, J. Magn. Magn. Mater. **185**, 274 (1998).
[19] C. Busse, S. Baud, G. Bihlmayer, C. Polop, T. Michely, and S. Blügel, Phys. Rev. B **68**, 201401(R) (2003).
[20] C. Busse and T. Michely, Surf. Sci. **552**, 281 (2004).
[21] H. L. Meyerheim, D. Sander, R. Popescu, J. Kirschner, O. Robach, S. Ferrer, and P. Steadman, Phys. Rev. B **67**, 155422 (2003).